

A PLASTIC-DAMAGE CONCRETE MODEL FOR EARTHQUAKE ANALYSIS OF DAMS

JEEHO LEE AND GREGORY L. FENVES*

Department of Civil and Environmental Engineering, University of California, Berkeley, Berkeley, CA 94720, U.S.A.

SUMMARY

A new plastic-damage constitutive model for cyclic loading of concrete has been developed for the earthquake analysis of concrete dams. The rate-independent model consistently includes the effects of strain softening, represented by separate damage variables for tension and compression. A simple scalar degradation model simulates the effects of damage on the elastic stiffness and the recovery of stiffness after cracks close. To simulate large crack opening displacements, the evolution of inelastic strain is stopped beyond a critical value for the tensile damage variable. Subsequent deformation can be recovered upon crack closing. The rate-independent plastic-damage model forms the backbone model for a rate-dependent viscoplastic extension. The rate-dependent regularization is necessary to obtain a unique and mesh objective numerical solution. Damping is represented as a linear viscoelastic behaviour proportional to the elastic stiffness including the degradation damage. The plastic-damage constitutive model is used to evaluate the response of Koyna dam in the 1967 Koyna earthquake. The analysis shows two localized cracks forming and then joining at the change in geometry of the upper part of the dam. The upper portion of the dam vibrates essentially as rigid-body rocking motion after the upper cracks form, but the dam remains stable. The vertical component of ground motion influences the post-cracking response. © 1998 John Wiley & Sons, Ltd.

KEY WORDS: concrete model; plastic damage; non-linear analysis; stiffness degradation; earthquake analysis; concrete dams

1. INTRODUCTION

Concrete gravity dams are expected to retain the water impounded in the reservoir during a safety evaluation earthquake. Although damage to the concrete in the form of limited cracking is acceptable, cracking cannot be extensive enough to cause instability of the dam structure and loss of the reservoir. Most dam safety evaluations currently utilize a linear elastic model for mass concrete in conjunction with criteria based on an allowable maximum tensile stress.¹ A linear earthquake analysis of a gravity dam subjected to strong ground motion invariably gives peak tensile stresses greater than the dynamic tensile strength of concrete. From such results *ad hoc* arguments about the duration and extent of large tensile stresses are used to justify dam safety, but it is difficult to ascertain the amount of damage and stability of a dam from a linear analysis.

Earthquake-induced damage of concrete dams has been examined experimentally by small-scale models on earthquake simulators.^{2,3} Although small-scale model tests present difficult issues of similitude, they have shown that a discrete crack forms near the upper portion of the upstream face and propagates to the downstream face, but that the dam remains stable after the earthquake. To date, the only gravity dam damaged more than superficially during an earthquake is Koyna dam in the 1967 Koyna earthquake.⁴ Several monoliths sustained horizontal cracks at the upstream and downstream faces. Contrary to the scale

* Correspondence to: Gregory L. Fenves, Department of Civil and Environmental Engineering, University of California-Berkeley, MC 1710, Berkeley, CA 94720, U.S.A. E-mail: fenves@ce.berkeley.edu

model tests, the cracking was somewhat distributed over the faces, but the depths of the cracks were not investigated.

Although field evidence of damage is limited, Hall³ emphasizes that no large dam with full reservoir has been subjected to a large, long duration earthquake at a small epicentral distance. A U.S. National Research Council⁵ report identified the nonlinear modeling of concrete as an important research need to assess the earthquake safety of dams. Since then researchers have made advances utilizing two different approaches. One approach uses fracture mechanics concepts to model the discrete cracking observed in plain concrete. When the discrete crack method is implemented using the finite element method, the domain is remeshed as the crack surface changes.⁶ While this is a viable numerical method for slowly applied loads, such as due to temperature and gravity, the computational effort is very large for dynamic analysis of earthquake response.

As a consequence, recent developments have utilized continuum models because of the ease of implementation using standard finite element analysis procedures. Early fixed smeared crack models for dams⁷⁻⁹ represented the fracture process zone by replacing the isotropic elastic constitutive relations with orthotropic properties. For the most part these models attempt to provide mesh objective solutions using a softening modulus related to the characteristic length of an element and the fracture energy for concrete, as originally formulated by Bazant and Oh.¹⁰ Disadvantages of the fixed smeared crack approach are arbitrariness of the shear retention factor and a build-up of shear stresses along the fixed crack surface causing the violation of the tension cut-off criterion.^{11,12}

An improved smeared crack approach, called the co-axial rotation crack model, was applied by Bhattacharjee and Léger¹³ to the earthquake analysis of dams. Softening is represented by a secant stiffness in the direction of maximum principal strain, and crack closing is represented by modifying the softening parameters based on the strain. Viscous damping is based on the tangent stiffness to represent energy dissipation. As applied to Koyna dam the earthquake analysis shows cracks at the downstream face, initiated at the change in slope, and at the base. However, in spite of many improvements on the smeared crack approach, it is still difficult to define rigorous evolution rules for a failure surface under multi-axial cyclic loading conditions and to model cracking with other inelastic phenomena near the fracture process zone.¹²

In contrast with the smeared crack approach, several researchers have used continuum damage mechanics to model concrete behaviour for dams. For clarity in the following presentation, continuum damage represented by stiffness degradation is called degradation damage, as opposed to the more general concept of damage which characterizes both the degradation of the elastic stiffness and the evolution of the elastoplastic yield surface. The fundamental aspect of continuum damage mechanics is the definition of an effective stress that represents the mapped stress into the microcracked (or damaged) surface. Ghrib and Tinawi¹⁴ developed an orthotropic damage model in which the damage evolution, loading/unloading conditions, and crack opening/closing rules are based on the total strain. This approach for inelastic constitutive models often requires *ad hoc* threshold rules and calibration factors with little physical meaning. Furthermore, it is difficult to justify the constitutive relationship between the principal stresses and modified total strains because the principal axes of the stress and modified total strain, which is typically defined as the difference between the total strain and initial threshold strain, do not coincide with each other. Addressing concerns about thermodynamic consistency and anomalous behaviour during opening and closing of crack under cyclic loads, Cervera *et al.*¹⁵ developed an isotropic damage model. The isotropic model accounts for the different behaviour of concrete in tension and compression by splitting the stress tensor into tension and compression components, each with its own damage surface and evolution law. The rate-independent model was then extended to account for rate dependency,¹⁶ which also provides the benefit of regularizing the ill-posed localization problem for strain-softening materials. The analysis of a dam similar to Koyna shows a significant reduction in the degradation damage because of the rate dependency. They found substantially similar earthquake response with the rate-independent model by increasing the tensile strength and fracture energy of concrete by 45 per cent.

Using continuum damage mechanics only, such as Cervera *et al.*,^{15,16} it is difficult to model cyclic loading and unloading states because there is no representation of the inelastic strain. Therefore, it is natural to

combine a classical damage model with plasticity models to overcome this shortcoming. In addition to the inelastic strain, the plastic-damage approach also provides well-defined evolution of the failure surface evolution and combination with other inelastic phenomena. Among several plastic-damage models, the model proposed by Lee and Fenves¹⁷ provides a simple and effective approach for the analysis of cyclically loaded concrete structures.

The paper first presents the overview of the plastic-damage model¹⁷ and its extension for large crack opening and closing. A simple and thermodynamically consistent scalar degradation model simulates the effects of damage on elastic stiffness and recovery. The rate-independent constitutive model is extended for viscoplastic rate-dependence as required for regularization of ill-posed transient boundary value problems. A new viscoelastic damping model, which is proportional to the degradation damage, is developed to prevent artificial damping forces at the crack surfaces. Finally, the constitutive model is applied to the earthquake analysis of a monolith of Koyna dam, demonstrating that damage, degradation, and stability of a dam can be evaluated in a thorough and rational manner.

2. PLASTIC-DAMAGE CONSTITUTIVE MODEL FOR CONCRETE

In the model proposed by Lee and Fenves¹⁷ the plastic-damage model by Lubliner *et al.*¹⁸ (called the Barcelona model) is extended to include two damage variables, one for tensile damage and the other for compressive damage, to account for several damage states. The uniaxial strength functions are factorized into two parts to represent the effective stress and degradation of elastic stiffness (degradation damage). The elastoplastic response is decoupled from the degradation damage response, leading to a relatively straightforward numerical implementation. A simple and thermodynamically consistent degradation recovery scheme is introduced to simulate cracking closing and re-opening. The rate-independent, plastic-damage constitutive model is fully described in Reference 17, but the salient aspects of the model for dam analysis are summarized in this section. A new approach for representing a large amount of crack opening and closing is described.

2.1. Constitutive relationships

In the incremental theory of plasticity, the strain tensor, $\boldsymbol{\varepsilon}$, is decomposed into the elastic part, $\boldsymbol{\varepsilon}^e$, and the plastic part, $\boldsymbol{\varepsilon}^p$, which for linear elasticity is given by

$$\begin{aligned}\boldsymbol{\varepsilon} &= \boldsymbol{\varepsilon}^e + \boldsymbol{\varepsilon}^p \\ \boldsymbol{\varepsilon}^e &= \mathbf{E}^{-1} : \boldsymbol{\sigma}\end{aligned}\quad (1)$$

where the elastic stiffness \mathbf{E} is a rank-four tensor, and $\boldsymbol{\sigma}$ is the stress tensor. Since the effective stress $\bar{\boldsymbol{\sigma}}$ is defined with the undamaged elastic stiffness from equation (1), it becomes

$$\bar{\boldsymbol{\sigma}} = \mathbf{E}_0 : (\boldsymbol{\varepsilon} - \boldsymbol{\varepsilon}^p) \quad (2)$$

where \mathbf{E}_0 is the initial elastic stiffness tensor. Scalar degradation damage, such that $\mathbf{E} = (1 - D)\mathbf{E}_0$, is assumed in many cases. Accordingly, the stress is factorized into stiffness degradation and effective stress parts:

$$\begin{aligned}\boldsymbol{\sigma} &= (1 - D)\bar{\boldsymbol{\sigma}} \\ &= (1 - D)\mathbf{E}_0 : (\boldsymbol{\varepsilon} - \boldsymbol{\varepsilon}^p)\end{aligned}\quad (3)$$

The plastic strain rate is evaluated by the flow rule, which is defined by a scalar plastic potential function, Φ . For a plastic potential in the effective stress space, the plastic strain is given by

$$\dot{\boldsymbol{\varepsilon}}^p = \dot{\lambda} \nabla_{\boldsymbol{\sigma}} \Phi(\bar{\boldsymbol{\sigma}}) \quad (4)$$

where $\dot{\lambda}$ is a non-negative function referred to as the plastic consistency parameter. In contrast with metals, a non-associative flow rule is necessary to obtain the proper dilatancy exhibited by frictional materials.¹⁹ A Drucker–Prager-type function is used as the plastic potential function:

$$\Phi = \|\mathbf{s}\| + \alpha_p I_1 \quad (5)$$

where, $I_1 = \text{tr}(\bar{\boldsymbol{\sigma}})$, and $\|\mathbf{s}\| = \sqrt{\mathbf{s}:\mathbf{s}}$ denotes the norm of the deviatoric effective stress, \mathbf{s} . The parameter α_p is chosen to give the proper dilatancy for concrete. The plastic strain rate is obtained from equations (4) and (5):

$$\dot{\boldsymbol{\epsilon}}^p = \dot{\lambda} \left(\frac{\mathbf{s}}{\|\mathbf{s}\|} + \alpha_p \mathbf{I} \right) \quad (6)$$

Another internal variable set, besides the plastic strain, is needed to represent the damage states. The damage variable, $\boldsymbol{\kappa}$, is assumed to be the only necessary state variable and its evolution is expressed as

$$\dot{\boldsymbol{\kappa}} = \dot{\lambda} \mathbf{H}(\bar{\boldsymbol{\sigma}}, \boldsymbol{\kappa}) \quad (7)$$

For modelling the cyclic behaviour of concrete, which has very different tensile and compressive yield strengths, it is necessary to use two cohesion variables in the yield function: c_t , a tensile cohesion variable, and c_c , a compressive cohesion variable. The yield function in the Barcelona model which only includes isotropic hardening in the classical plasticity sense, is modified to include two cohesion variables:

$$F(\bar{\boldsymbol{\sigma}}, \boldsymbol{\kappa}) = \frac{1}{1-\alpha} [\alpha I_1 + \sqrt{3J_2} + \beta(\boldsymbol{\kappa}) \langle \hat{\sigma}_{\max} \rangle] - c(\boldsymbol{\kappa}), \quad (8)$$

where $\hat{\sigma}_{\max}$ denotes the algebraically maximum principal stress, and α is a parameter which is evaluated by the initial shape of the yield function. The evolution of the yield function is determined by defining β , which is a constant in the Barcelona model, and the cohesion parameter, c , such that

$$\begin{aligned} \beta &= \frac{c_c(\boldsymbol{\kappa})}{c_t(\boldsymbol{\kappa})} (1 - \alpha) - (1 + \alpha) \\ c &= c_c(\boldsymbol{\kappa}) \end{aligned} \quad (9)$$

Figure 1 shows the initial shape of the yield surface, $F(\bar{\boldsymbol{\sigma}}, \mathbf{0}) = 0$, in the principal plane stress space. In Figure 1, β_0 and c_0 denote β and c , respectively, at the undamaged initial state.

2.2. Evolution of damage

To model the different damage states for tensile and compressive loading, both κ_t and κ_c are used as independent damage variables, and $\boldsymbol{\kappa}$ is defined as

$$\boldsymbol{\kappa} = \begin{bmatrix} \kappa_t \\ \kappa_c \end{bmatrix} \quad (10)$$

The evolution equations for the hardening and degradation variables are obtained from the factorization of the uniaxial stress strength function, $f_{\aleph} = f_{\aleph}(\kappa_{\aleph})$, such that

$$f_{\aleph} = (1 - D_{\aleph}) \bar{f}_{\aleph} \quad (11)$$

where $\aleph \in \{t, c\}$ is a state variable such that the state is uniaxial tensile if \aleph is t and uniaxial compressive if \aleph is c . Accordingly, the effective stress $\bar{\sigma}_{\aleph}$ and degradation damage variable D_{\aleph} are defined as functions of κ_{\aleph} :

$$\bar{\sigma}_{\aleph} = \bar{f}_{\aleph}(\kappa_{\aleph}) \quad (12)$$

$$D_{\aleph} = D_{\aleph}(\kappa_{\aleph}) \quad (13)$$

in which $0 \leq D_{\aleph} < 1$ and $\dot{D}_{\aleph} \geq 0$. The relation in equation (12) describes the evolution of the cohesion variable used in the yield function, and equation (13) defines the degradation damage as a function of the damage variable.

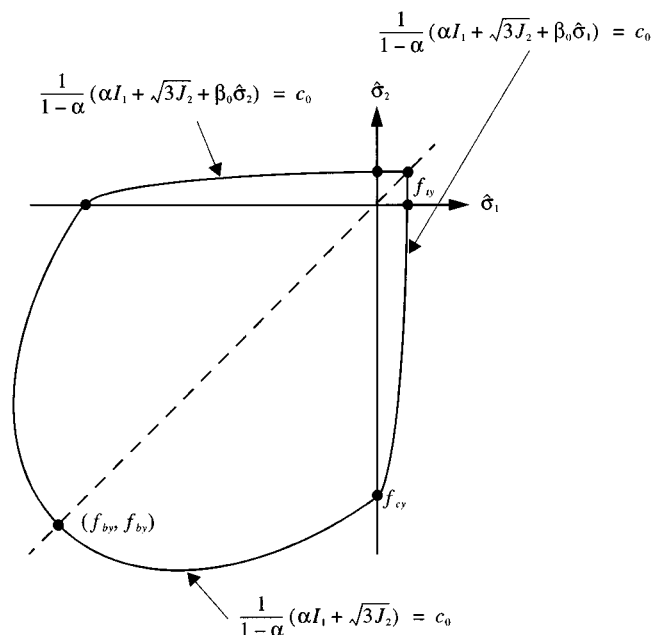


Figure 1. Initial yield function in plane stress space

The damage evolution for a uniaxial state is defined based on the dissipated plastic energy, which can be written for quasi-brittle materials as

$$\dot{\kappa}_{\text{N}} = \frac{1}{g_{\text{N}}} f_{\text{N}}(\kappa_{\text{N}}) \dot{\varepsilon}^{\text{p}} \quad (14)$$

where g_{N} is the energy capacity per unit volume of materials. To maintain objective results at the structural level, the crack bandwidth along which the energy is dissipated is specified as a material property as $g_{\text{N}} = G_{\text{N}}/l_{\text{N}}$,^{18,20} where G_{N} is the fracture energy in the uniaxial state and its counterpart in the uniaxial compressive state, and l_{N} is the characteristic length representing the crack bandwidth.

The evolution equation in equation (14) can be generalized for multiaxial cases in the form of

$$\dot{\kappa} = \dot{\lambda} \hat{\mathbf{H}}(\hat{\boldsymbol{\sigma}}, \kappa) \quad (15)$$

where $\hat{\mathbf{H}} = \mathbf{h}(\hat{\boldsymbol{\sigma}}, \kappa) \cdot \nabla_{\hat{\boldsymbol{\sigma}}} G(\hat{\boldsymbol{\sigma}})$. Equation (15) is the specific form of evolution in equation (7) for the damage variables in terms of the effective stress and damage variables themselves.

2.3. Stiffness degradation and crack opening/closing

The experimental cyclic tests of concrete demonstrate that the degradation of stiffness from microcracking occurs in tension and compression becomes more significant as the strain increases. The mechanism of stiffness degradation under cyclic loading is complicated because of the opening and closing of microcracks. The crack opening/closing behaviour can be modelled as elastic stiffness recovery during elastic unloading from a tensile state to a compressive state. The degradation damage variable defined in equation (13) is modified by a multiplicative parameter, $0 < s < 1$, on D :

$$D = 1 - (1 - D_{\text{c}}(\kappa))(1 - sD_{\text{t}}(\kappa)) \quad (16)$$

The parameter $s = s(r(\hat{\sigma}))$ represents stiffness recovery because r is a weight function of the effective stress, which ranges from zero in pure compressive loading to unity in pure tensile loading. Substituting equation (16) into equation (3) gives the total stress:

$$\boldsymbol{\sigma} = (1 - D_c(\boldsymbol{\kappa}))(1 - sD_t(\boldsymbol{\kappa}))\mathbf{E}_0 : (\boldsymbol{\varepsilon} - \boldsymbol{\varepsilon}^p) \quad (17)$$

After a large amount of microcracking, the crack opening and closing mechanism becomes similar to discrete cracking, which cannot be represented by the classical approach of inelastic strain evolution. A modified evolution relation is used to simulate large crack opening and the closing/reopening process in the continuum context. It can be assumed that the microcracks are joined to construct a discrete crack if $\kappa_t \geq \kappa_{cr}$, where κ_{cr} is an empirical value near unity. At that tensile damage level, the evolution of the plastic strain caused by the tensile damage is stopped and the plastic strain rate is defined by an intermediate effective stress $\tilde{\boldsymbol{\sigma}}$:

$$\begin{aligned} \tilde{\boldsymbol{\sigma}} &= \mathbf{E}_0 : (\boldsymbol{\varepsilon} - \tilde{\boldsymbol{\varepsilon}}^p) \in \{\tilde{\boldsymbol{\sigma}} | F(\tilde{\boldsymbol{\sigma}}, \boldsymbol{\kappa}) \leq 0\} \\ \dot{\tilde{\boldsymbol{\varepsilon}}}^p &= \dot{\lambda} \nabla_{\tilde{\boldsymbol{\sigma}}} \Phi(\tilde{\boldsymbol{\sigma}}) \\ \bar{\boldsymbol{\sigma}} &= \mathbf{E}_0 : (\boldsymbol{\varepsilon} - \boldsymbol{\varepsilon}^p) \\ \dot{\boldsymbol{\varepsilon}}^p &= (1 - r(\hat{\boldsymbol{\sigma}})) \dot{\lambda} \dot{\tilde{\boldsymbol{\varepsilon}}}^p \end{aligned} \quad (18)$$

With the relations in equation (18), the degradation variable in equation (16) is redefined as

$$D = 1 - (1 - D_c(\boldsymbol{\kappa}))(1 - sD_t(\boldsymbol{\kappa}))(1 - sD_{cr}) \quad (19)$$

where $0 \leq D_{cr} < 1$ is an additional degradation variable and determined by the Kuhn–Tucker–type loading/unloading conditions such that

$$\begin{aligned} \dot{D}_{cr} &\geq 0 \\ \dot{D}_{cr} F((1 - D_{cr})\bar{\boldsymbol{\sigma}}, \boldsymbol{\kappa}) &= 0 \\ F((1 - D_{cr})\bar{\boldsymbol{\sigma}}, \boldsymbol{\kappa}) &\leq 0 \end{aligned} \quad (20)$$

During continued loading ($\dot{D}_{cr} > 0$), $F((1 - D_{cr})\bar{\boldsymbol{\sigma}}, \boldsymbol{\kappa}) = (1 - D_{cr})(F(\bar{\boldsymbol{\sigma}}, \boldsymbol{\kappa}) + c_c) - c_c = 0$ which leads to

$$D_{cr} = 1 - \frac{c_c}{(F(\bar{\boldsymbol{\sigma}}, \boldsymbol{\kappa}) + c_c)} \quad (21)$$

It is noted that $(F(\bar{\boldsymbol{\sigma}}, \boldsymbol{\kappa}) + c_c)$ is a first-degree homogeneous function with respect to $\bar{\boldsymbol{\sigma}}$.

Thermodynamic consistency of the model including the new degradation variable can be ensured by redefining ω in the generalized Helmholtz free energy rate $\dot{\Psi} = \dot{e} - \omega \boldsymbol{\sigma} : \dot{\boldsymbol{\varepsilon}} - \rho \dot{\eta} \theta - \rho \eta \dot{\theta}$, in which e is the internal energy per unit volume, ρ is the density, η is the entropy per unit mass and θ is the thermodynamic temperature, from Lee and Fenves¹⁷ as

$$\omega = 1 - (1 - \omega_1)(1 - \omega_2) \quad (22)$$

where $\omega_1 = (1 - s)D_t/(1 - sD_t)$ and $\omega_2 = (1 - s)D_{cr}/(1 - sD_{cr})$. It is noted that $0 \leq \omega < 1$ because $0 \leq \omega_1, \omega_2 < 1$. The relation between the Helmholtz free energy and the total potential energy function of an undamaged material, Ψ_0 , is defined as $\Psi = (1 - \tilde{d})\Psi_0$, in which $\tilde{d} = 1 - (1 - D_c)(1 - D_t)(1 - D_{cr})$. Because $\tilde{d} \geq 0$, and it can be assumed that $(\partial\Psi_0/\partial\boldsymbol{\kappa}) \cdot \dot{\boldsymbol{\kappa}} \leq 0$ as shown in Reference 17, thermodynamic consistency of the present model is obtained by introducing Ψ_0 such that $\partial\Psi_0/\partial\boldsymbol{\varepsilon}^e = \mathbf{E}_0 : \boldsymbol{\varepsilon}^e$, which leads the relation

$$\boldsymbol{\sigma} = \frac{(1 - \tilde{d})}{(1 - \omega_1)(1 - \omega_2)} \frac{\partial\Psi_0}{\partial\boldsymbol{\varepsilon}^e} \quad (23)$$

to become identical to equation (3) using equation (19).

2.4. Cyclic loading examples

A numerical algorithm for the rate-independent plastic-damage model has been developed²¹ and implemented as a part of the finite element program FEAP.²² Several applications of the numerical model for cyclically loaded concrete tests are presented in this section using a single four-node plane stress quadrilateral isoparametric elements. The loads are applied by displacement control, and for all cases Poisson's ratio is 0.18.

To compare the rate-independent model with the existing experimental results,^{23,24} the following material properties are used: (1) for cyclic tensile case, $E_0 = 3.17 \times 10^4$ MPa, $f'_t = 3.48$ MPa, $G_t = 40$ N/m, $l_t = 82.6$ mm, $\alpha_p = 0.2$; and (2) for cyclic compressive case, $E_0 = 3.1 \times 10^4$ MPa, $f'_c = -27.6$ MPa, $G_c = 5690$ N/m, $l_c = 82.6$ mm, $\alpha_p = 0.2$. Figure 2 shows the simulated tensile and compressive stress-strain behaviours, respectively. The numerical simulations represent the experimental results very well. For both cases the degradation of stiffness is simulated at each unloading/reloading cycle as well as the softening behaviour. The hysteresis on reloading cannot be simulated by the model because of the rate-independent elastic loading/unloading assumption.

As another example, cyclic loading under large tension and compression strains is imposed on a single element patch with the material properties: $E_0 = 3 \times 10^4$ MPa, $f'_t = 2.5$ MPa, $f'_c = -25$ MPa, $G_t = 180$ N/m, $G_c = 18\,000$ N/m, $l_t = 1$ m, $l_c = 1$ m, $\alpha_p = 0.2$. The result is illustrated in Figure 3 with the loading path A-B-C-D-E-F-G. During the tensile unloading-compressive loading path (path A-B and path D-E-F), the stiffness is recovered. The compressive strength after tensile loading is not degraded (path A-B), which means that the compressive damage is not affected by the tensile damage. On the other hand, the tensile strength depends on the compressive load path because the stiffness degradation from compressive damage is not recovered during tensile unloading (path B-C). This is physically reasonable, because the compressive failure is mainly caused by dilatancy, which affects the subsequent compressive and tensile strengths. Large crack opening and closing is simulated during path C-D-E. The crack closes at Point E and the elastic stiffness is recovered, yielding in compression again to reach point F. Reopening of the crack is shown along path F-G after unloading.

3. EXTENSIONS FOR RATE-DEPENDENT MODEL

In contrast with metals, inelastic behaviour of concrete is characterized by softening with increased strain. Hence, the modeling of softening as well as hardening behaviour is important for realistic static and dynamic analyses of concrete structures. Unfortunately, representing the softening behaviour with a model based on rate-independent plasticity makes the governing initial-boundary value problem become ill-posed such that a unique solution may not exist.²⁵⁻²⁸ In most cases, uniqueness is not guaranteed in softening regions and, with a non-associative flow rule, even in hardening regions. A numerical solution for an ill-posed initial-boundary value problem cannot guarantee a unique converged solution and the results show a strong dependency on mesh refinement and alignment. Since a rate-independent plasticity model is constrained by the plastic consistency condition, it gives a singularity in the plastic multiplier. This singularity can be regularized using viscoplasticity by permitting stresses to be outside of the yield surface. The rate-independent plastic model is assumed to be a limit state of the corresponding viscoplastic model. In this section, a rate-dependent version of the plastic-damage model is developed by introducing a viscoplastic concept into the inelastic strain and degradation variable.

3.1. Rate-dependent regularization

Two well-known viscoplastic models used for regularization are the Perzyna model²⁹ and the Duvaut-Lions model.³⁰ The Duvaut-Lions model is more appropriate for the regularization of a

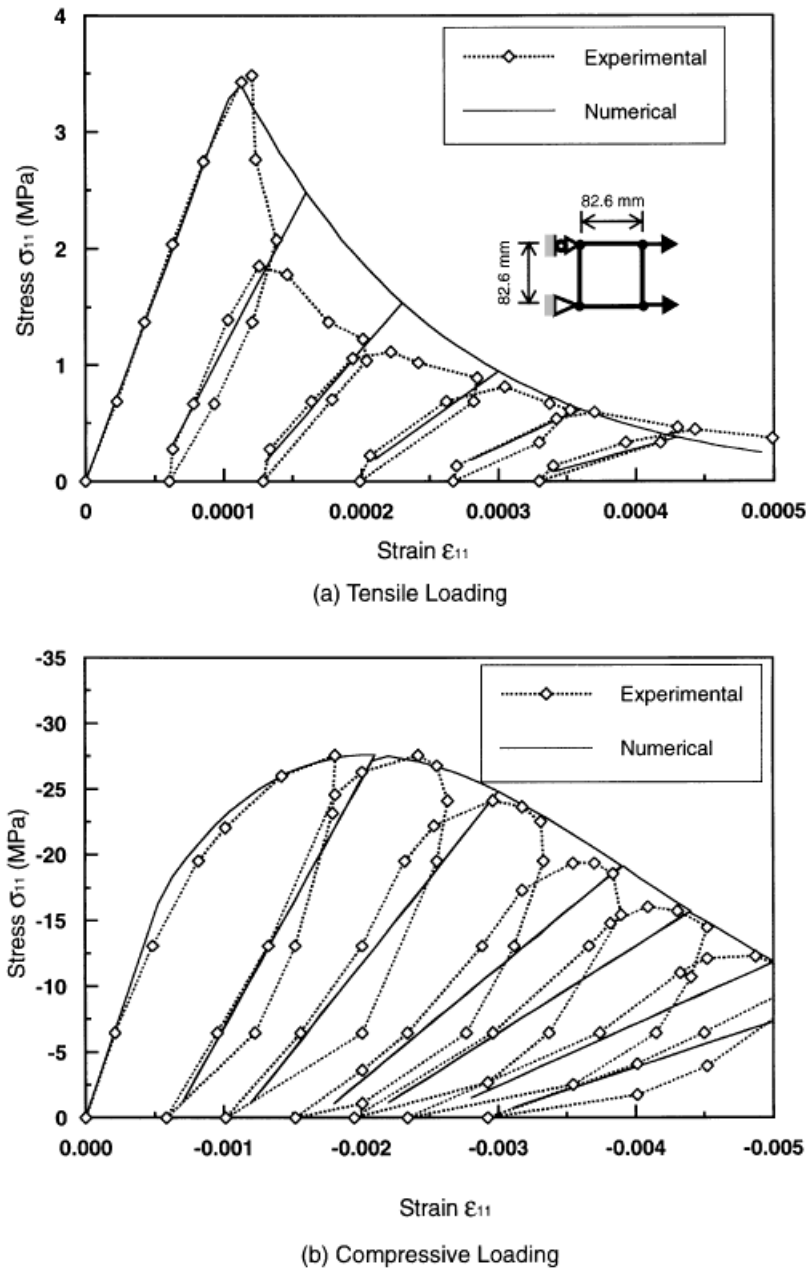


Figure 2. Numerical simulation of cyclic uniaxial loading compared with experimental results

rate-independent plastic-damage model, because the Perzyna model fails to converge to the rate-independent backbone model in some cases.³¹ In the original Duvaut–Lions model, inelastic strain rate, $\dot{\epsilon}^i$, is defined as

$$\dot{\epsilon}^i = \frac{1}{\mu} \mathbf{E}^{-1} : (\boldsymbol{\sigma} - \boldsymbol{\sigma}^*) \quad (24)$$

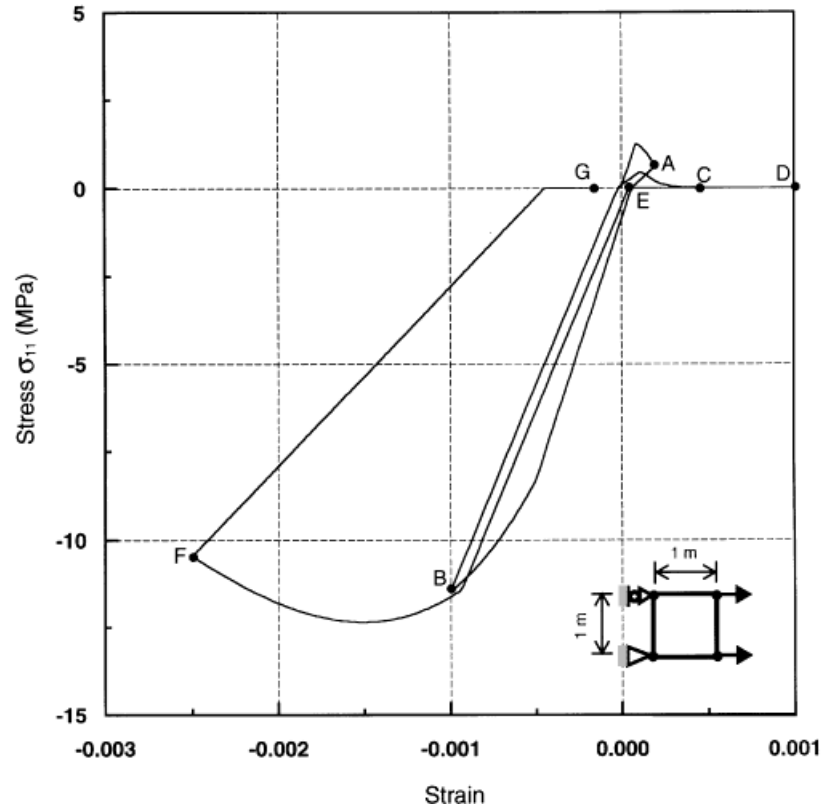


Figure 3. Numerical simulation of cyclic crack opening and closing

where σ^* denotes the projection of the stress, σ , on a yield surface, and μ , which is called the viscosity parameter, represents the relaxation time of the viscoplastic system. The original Duvaut–Lions model can be generalized for any backbone model, regardless of the existence of the projection on a yield surface, by defining σ^* to be the stress of the rate-independent backbone model for the current strain ϵ .

Using the cyclic plastic-damage model as the backbone model, equation (24) is rewritten as

$$\dot{\epsilon}^i = \frac{1}{\mu} \mathbf{E}^{-1} : [\sigma - (1 - D)\bar{\sigma}] \quad (25)$$

where $\bar{\sigma}$ is the effective stress, which is evaluated in the rate-independent backbone model. The stress–strain relation is

$$\begin{aligned} \sigma &= \mathbf{E} : (\epsilon - \epsilon^i) \\ \mathbf{E} &= (1 - D)\mathbf{E}_0 \end{aligned} \quad (26)$$

With equations (3) and (26), the inelastic strain rate in equation (25) becomes

$$\dot{\epsilon}^i = \frac{1}{\mu} (\epsilon^p - \epsilon^i) \quad (27)$$

Similarly, a rate-dependent degradation damage variable D is defined such that

$$\dot{D} = \frac{1}{\mu}(\bar{D} - D) \quad (28)$$

where \bar{D} is the degradation damage variable defined in the rate-independent model, which is described in Section 2.

Equations (26)–(28) constitute the viscoplastic model based on the rate-independent backbone model. To show this model gives a unique solution in the incremental sense, consider two admissible stress rate fields:

$$\begin{aligned} \Delta \dot{\sigma} &= \Delta(\mathbf{E} : (\dot{\epsilon} - \dot{\epsilon}^i)) - \Delta(\dot{D} \mathbf{E}_0 : (\epsilon - \epsilon^i)) \\ &= \mathbf{E} : \Delta \dot{\epsilon} - \mathbf{E} : \Delta \dot{\epsilon}^i - \Delta(\dot{D}) \mathbf{E}_0 : (\epsilon - \epsilon^i) \\ &= \mathbf{E} : \Delta \dot{\epsilon} \end{aligned} \quad (29)$$

where Δ denotes a difference between two admissible fields. In equation (29), the differences between two possible inelastic strain rates and degradation rates vanish, because they are determined by the current values³² as in equations (27) and (28). Since \mathbf{E} is a positive-definite tensor, equation (29) gives

$$\Delta \dot{\sigma} : \Delta \dot{\epsilon} = \Delta \dot{\epsilon} : \mathbf{E} : \Delta \dot{\epsilon} > 0 \quad (30)$$

unless or $\Delta \dot{\epsilon} = 0$ or $\Delta \dot{\sigma} = 0$. Therefore, the incremental uniqueness criterion^{32,33} is satisfied, which implies that the incremental stress field is unique in the model.

In the rate-dependent model, the characteristic length mentioned in Section 2.2 is related to the crack bandwidth. It can be determined from the internal length scale regardless of the finite element mesh for problems dominated by the high-frequency response.^{21,34,35} On the other hand, for quasi-static or relatively low-frequency problems, such as earthquake response, the element size is an important factor to include in the characteristic length because the rate-dependent regularization effect becomes weaker. With μ set to 15 per cent of the time step, it is recommended to use the element size directly as the characteristic length, l_∞ , for quasi-static or low frequency problems based on a numerical parametric study.²¹

4. NON-LINEAR EARTHQUAKE ANALYSIS OF CONCRETE DAMS

The earthquake response of concrete gravity dams is affected by dam–water interaction and dam–foundation interaction.¹ Although the interaction effects can be rigorously included in a frequency-domain analysis for a linear model,³⁶ a time domain analysis is necessary for nonlinear models. The purpose of the present work is to demonstrate the plastic-damage constitutive model described in Sections 2 and 3, so dam–water interaction effects are included by an added mass for incompressible water, as in several earlier studies.^{13,14} Dam–foundation interaction is neglected by assuming the foundation rigid, which is not unrealistic for the rock at the Koyna site.⁴ Vector–matrix notation is used in this section.

The equations of motion for the discretized dam for specified free-field ground acceleration are

$$\mathbf{M}\ddot{\mathbf{u}} + \mathbf{P}(\mathbf{u}, \dot{\mathbf{u}}) = -\mathbf{M}\mathbf{R}\ddot{\mathbf{u}}_g + \mathbf{F}^{\text{st}} \quad (31)$$

where \mathbf{u} , $\dot{\mathbf{u}}$, and $\ddot{\mathbf{u}}$ are the displacement, velocity, and acceleration relative to the free-field ground motion, $\ddot{\mathbf{u}}_g$; \mathbf{M} is the mass matrix including the added mass for the reservoir, \mathbf{P} is the restoring forces obtained from the finite element discretization, \mathbf{R} is the influence matrix for $\ddot{\mathbf{u}}_g$, and \mathbf{F}^{st} are the static loads from self-weight of the dam and the hydrostatic pressure on the upstream face.

In the finite element analysis procedure, the restoring force \mathbf{P} is assembled from the element contributions. For each element the restoring force, \mathbf{P}_e , is given by the integral of the stress field in the element domain Ω_e , as governed by the rate-dependent constitutive model:

$$\mathbf{P}_e(\mathbf{u}, \dot{\mathbf{u}}) = \int_{\Omega_e} \mathbf{B}^T \boldsymbol{\sigma} d\Omega + \int_{\Omega_e} \mathbf{B}^T \boldsymbol{\chi} d\Omega \quad (32)$$

where \mathbf{B} is the matrix form of the strain-displacement operator, and χ is the contribution of the viscoelastic damping to the restoring stress.

4.1. Damping

From ambient and forced vibration testing of dams,³ it is generally assumed that dams have damping ratios of 2–5 per cent caused by energy dissipation in the concrete material. To represent damping, it is necessary to include a dissipative force in equation (32) because the rate-dependent model does not include a viscoelastic term. Viscoelastic energy dissipation can represent material damping, but it must be done a manner that does not affect the cracking patterns or affect the convergence of the numerical procedure for solving the equations of motion.

Considering an element, the damping stress can be represented as a linear viscoelastic term:

$$\chi(\dot{\epsilon}) = b_0 \mathbf{E}_0 \dot{\epsilon} \quad (33)$$

where b_0 is a coefficient calibrated to provide a damping ratio at one natural vibration period assuming undamaged material. Equation (33) simply represents stiffness proportional damping. The mass proportional damping term in the Rayleigh damping model is not included because it does not have a physical basis to justify it. As pointed out by El-Aidi and Hall,⁹ constant stiffness proportional damping introduces artificial damping forces as cracks open with large relative velocity and the damping forces then restrains the crack opening by transferring artificial stresses across the crack. To remedy this problem various investigators have set the damping term to zero upon cracking of an element or used a tangent stiffness matrix. However, these approaches may affect the stability of the numerical solution because damping forces change rapidly, and they can certainly reduce the convergence rate unless the viscoelastic damping is included in the consistent algorithmic tangent matrix.

In this work viscoelastic damping stress is based consistently on the elastic properties accounting for degradation damage:

$$\chi(\epsilon, \dot{\epsilon}) = b_0(1 - \bar{D}) \mathbf{E}_0 \dot{\epsilon} \quad (34)$$

where \bar{D} is the rate-independent degradation damage variable described in Section 2.3. As degradation damage evolves, the viscoelastic damping becomes smaller, which essentially eliminates damping forces in the damaged region. Upon crack closing, degradation damage is partially reduced and hence damping is restored. The damage-dependent damping defined in equation (34) can be included consistently in the algorithmic tangent matrix.

4.2. Numerical implementation

The discrete form of the equation of motion in equation (31) is written as³⁷

$$\mathbf{M}\ddot{\mathbf{u}}_{n+1} + \mathbf{P}(\mathbf{u}_{n+\varphi}, \dot{\mathbf{u}}_{n+\varphi}) = \mathbf{F}_{n+\varphi} \quad (35)$$

where $\mathbf{F} = -\mathbf{M}\mathbf{R}\ddot{\mathbf{u}}_g + \mathbf{F}^{\text{st}}$, $\mathbf{u}_{n+\varphi} = \varphi \mathbf{u}_n + (1 - \varphi) \mathbf{u}_{n+1}$, $\mathbf{F}_{n+\varphi} = \varphi \mathbf{F}_n + (1 - \varphi) \mathbf{F}_{n+1}$, and $0 < \varphi \leq 1$. With the Newmark formulation for the velocity and acceleration fields, equation (35) becomes the α -method³⁸ in linear elastodynamic problems. Linearization of equation (35) gives

$$\left(\mathbf{M} \frac{\partial \ddot{\mathbf{u}}_{n+1}}{\partial \mathbf{u}_{n+1}} + \frac{\partial \mathbf{P}}{\partial \mathbf{u}_{n+\varphi}} \frac{\partial \mathbf{u}_{n+\varphi}}{\partial \mathbf{u}_{n+1}} + \frac{\partial \mathbf{P}}{\partial \dot{\mathbf{u}}_{n+\varphi}} \frac{\partial \dot{\mathbf{u}}_{n+\varphi}}{\partial \mathbf{u}_{n+1}} \right) \Delta \mathbf{u} = \Delta \mathbf{F}_{n+\varphi} \quad (36)$$

Considering equation (34), the element contributions to the partial derivatives in equation (36) are

$$\begin{aligned} \frac{\partial \mathbf{P}_e}{\partial \mathbf{u}_{n+\varphi}} &= \int_{\Omega_e} \mathbf{B}^T (\mathbf{E}_{\text{alg}})_{n+\varphi} \mathbf{B} d\Omega \\ \frac{\partial \mathbf{P}_e}{\partial \dot{\mathbf{u}}_{n+\varphi}} &= \int_{\Omega_e} \mathbf{B}^T [b_0(1 - \bar{D}_{n+\varphi}) \mathbf{E}_0] \mathbf{B} d\Omega \end{aligned} \quad (37)$$

where \mathbf{E}_{alg} is a modified algorithmic tangent with the damping. The gradients, $\partial \ddot{\mathbf{u}}_{n+1} / \partial \mathbf{u}_{n+1}$, $\partial \mathbf{u}_{n+\varphi} / \partial \mathbf{u}_{n+1}$ and $\partial \dot{\mathbf{u}}_{n+\varphi} / \partial \mathbf{u}_{n+1}$, are constants determined by the integration scheme used for equation (35).

The consistent algorithmic tangent^{31,39} can be expressed in terms of the algorithmic tangent without the damping²¹ $(\partial \boldsymbol{\sigma}_{n+\varphi} / \partial \boldsymbol{\varepsilon}_{n+\varphi})_{\text{alg}}$ and the degradation damage variable, \bar{D} :

$$(\mathbf{E}_{\text{alg}})_{n+\varphi} = \left(\frac{\partial \boldsymbol{\sigma}_{n+\varphi}}{\partial \boldsymbol{\varepsilon}_{n+\varphi}} \right)_{\text{alg}} - \frac{\boldsymbol{\chi}_{n+\varphi} (\partial \bar{D}_{n+\varphi} / \partial \boldsymbol{\varepsilon}_{n+\varphi})^T}{(1 - \bar{D}_{n+\varphi})} \quad (38)$$

5. ANALYSIS OF DAMAGE TO KOYNA DAM

Koyna dam was damaged during a short duration earthquake ($M_s = 6.5$) on 11 December 1967, with an epicentral distance of 13 km. The dam is 850 m long and, as shown in Figure 4(a), a typical non-overflow monolith is 103 m high with the reservoir at a depth of 91.7 m at the time of the earthquake. The transverse and vertical acceleration records from an accelerograph in a gallery, shown in Figure 4(c) and 4(d), are considered representative of the free-field ground motion for the dam. Several monoliths had horizontal cracks between elevations 60 and 66 m at the upstream face and near elevation 66 m at the downstream face,⁴ although other maps of cracks have been documented.³ Damage to the dam has been investigated with a number of different nonlinear models and analysis procedures, several of which were described in Section 1. This section presents the earthquake analysis of Koyna dam using the new plastic-damage model for concrete implemented in FEAP.²² The finite element mesh of the dam, shown in Figure 4(b), uses 760 four-node plane stress quadrilateral isoparametric elements with 2×2 Gauss integration.

Although different concrete mixes were used in the dam construction, investigators have assumed similar material properties. For this study they are: $E_0 = 3.0 \times 10^4$ MPa, $\rho = 2630$ kg/m³, $\nu = 0.20$. Based on the compressive strength, $f'_c = -24.1$ MPa, for the concrete in the central portion of the dam, the tensile strength is estimated to be $f'_t = 2.41$ MPa. To account for strain rate effects, the tensile strength is increased by 20 per cent to a value of 2.90 MPa, since the strength increase is not included in the present rate-dependent regularization. The fracture energy is assumed to be $G_t = 200$ N/m. Each element size is used for both characteristic lengths l_t and l_c in the constitutive relations. The time step of $\Delta t = 0.005$ sec, the viscosity parameter $\mu = 0.15$, $\Delta t = 0.00075$ sec, and $\varphi = 0.5$ are selected for the time integration procedure. The time integration is performed for 15 sec, of which the last 5 sec is free vibration after the 10 sec of recorded ground motion. The stiffness damping parameter is $b_0 = 0.0033$ sec to provide 3 per cent damping at the fundamental vibration period $T_1 = 0.346$ sec. The full reservoir is represented by added masses at the upstream face nodal points.

Figure 5(a) shows the history of horizontal displacement at the dam crest, with positive displacement in the downstream direction, for the combined static and earthquake loads due to both components of the ground motion. The dashed line is the dam response assuming the concrete is linear elastic, whereas the solid line is the response of the dam using the plastic-damage model. For approximately the first four seconds the crest displacement is less than 30 mm and the maximum principal stress is less than the uniaxial tensile strength.

The first large excursion of the dam in the downstream direction occurs at 4.155 sec, marked as time A in Figure 5(a). Although the crest displacements for the linear model and plastic-damage model are similar up to this time, some damage has occurred as will be described later. The subsequent upstream excursion occurs at 4.375 sec (time B), for which the plastic-damage model gives an upstream displacement of 58 mm, which is about a 30 per cent greater than the displacement of the corresponding peak for the linear model. For tracking the damage evolution, the peak displacements at the next downstream excursion (4.580 sec, time C) and upstream excursion (4.860 sec, time D) are marked in Figure 5(a). It is clear from Figure 5(a) that the non-linear response has a substantially different displacement history than the linear model after time B. The apparent vibration period lengthens about 30 per cent to 0.465 sec compared with the linear first mode period. For the plastic-damage model, the crest displacement is dominated by rigid-body rocking of the

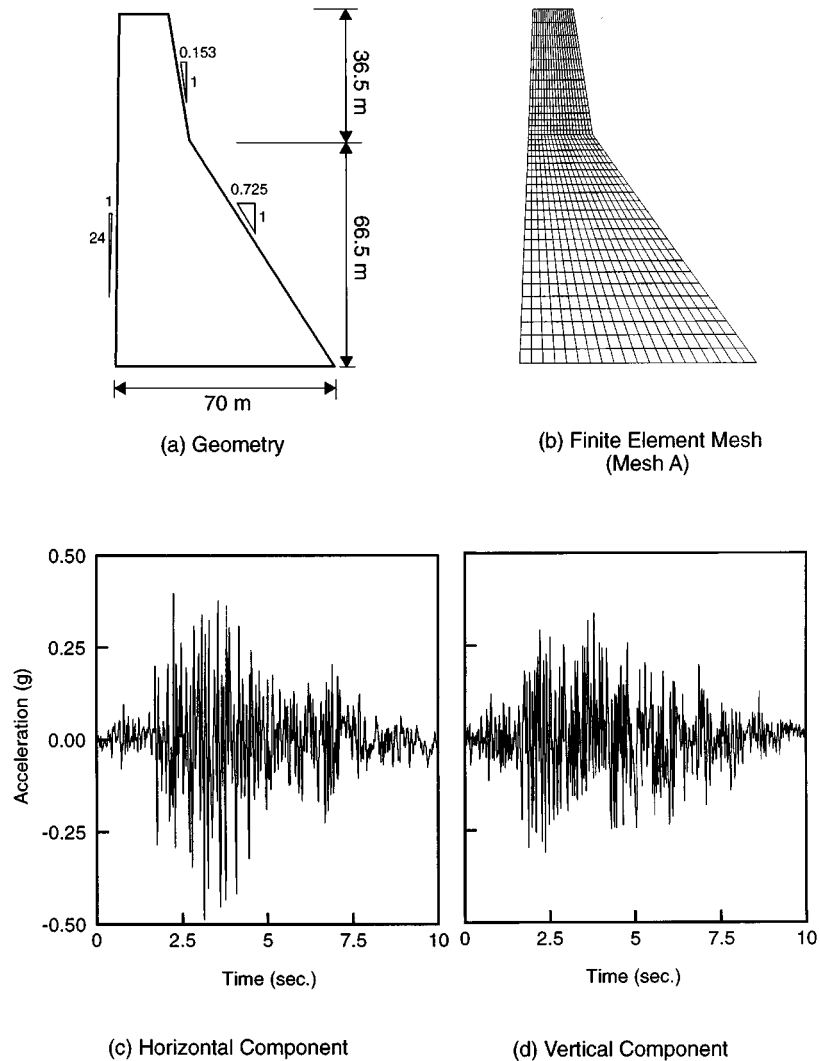
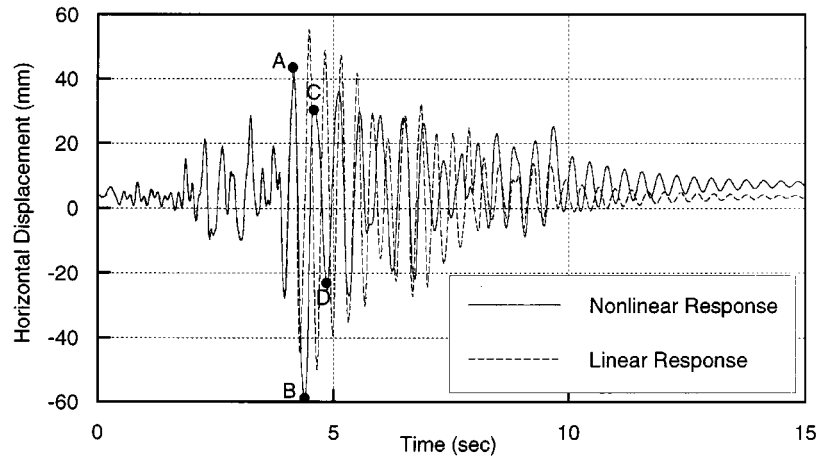


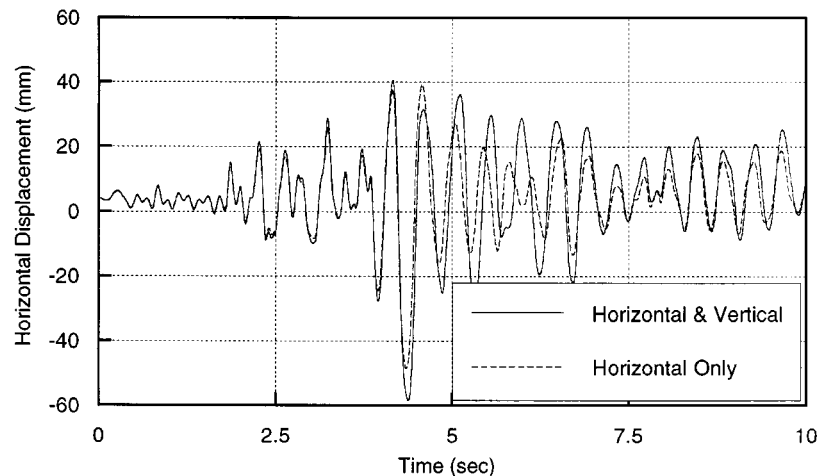
Figure 4. Geometry and mesh of Koyna Dam, and 1967 Koyna Earthquake ground motion components

upper portion of the dam after the formation of cracks near the change in downstream slope. At all times the nonlinear response analysis shows that the dam remains stable.

Before examining the damage evolution in the dam, Figure 5(b) shows the effect of the vertical ground motion component on the nonlinear displacement history at the crest. Prior to time B, when major cracking occurs, there is little difference between the displacement histories for the dam subjected to both ground motion components and the dam subjected to the horizontal component only. After time B, however, the response of the dam to both components has slightly larger amplitude oscillations at a longer vibration period than the response to the horizontal component only. A linear analysis of Koyna dam gives very similar crest displacement histories with the maximum displacement for both components about 10 per cent greater than the crest displacement due to the horizontal component only. The post-cracking response of the dam, however, is more sensitive to the vertical ground motion component than normally seen in linear



(a) Comparison of Linear and Nonlinear Responses with Horizontal and Vertical Ground Motion Components



(b) Effect of Vertical Ground Motion Component on Nonlinear Response

Figure 5. Horizontal displacement history at crest of Koyna Dam

models. The two components produce a crack pattern which allows essentially rigid body rotation of the upper part of the dam.

Returning to the plastic-damage model results for the dam subjected to both components of ground motion, Figures 6, 7, and 8 show the evolution of maximum principal stress, the tensile damage parameter, and the degradation damage parameter, respectively, at the four times indicated in the crest displacement history in Figure 5(a). At time A, Figure 6(a) shows two areas of tensile stresses greater than 0.5 MPa, at the

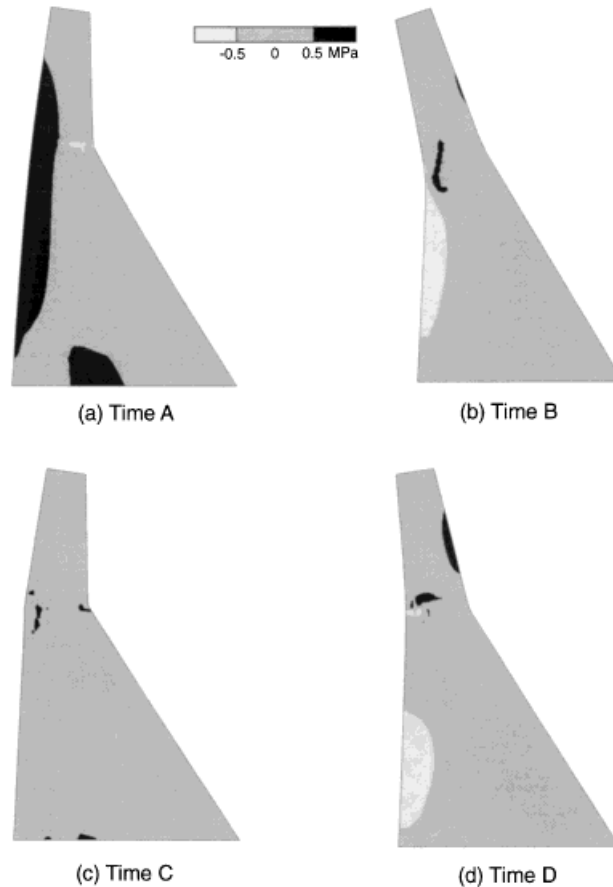


Figure 6. Deformed shapes and maximum principal stress contours

upstream face and near the middle of the base. The large upper region shows a typical stress contour due to bending of the monolith upstream, whereas the bottom contour is a stress concentration at the tip of the horizontal crack which has formed at the base. This interpretation is clarified by examining the damage contours at time A in Figures 7(a) and 8(a). Slight damage has developed near the middle of the upstream face, and a crack at the base has propagated from the upstream face into the dam about one-quarter of the base dimension. Furthermore, Figure 7(a) shows that prior to time A, a horizontal crack initiated at the downstream face near the stress concentration at the change in downstream slope. As shown in Figure 8(a) the degradation damage in this upper region recovers at time A because the previously formed upper crack is closed.

At time B, the first large upstream displacement excursion, Figure 6(b) shows that most of the crest displacement is rigid body rotation of the upper portion of the dam. The tensile stress contour in the middle of the dam is near the tip of the upper crack. Figures 7(b) and 8(b) show that the upper crack propagates to about one-half of the thickness at that elevation and then turns down at approximately a 30° angle to the vertical. The damaged zone is very localized, generally one element wide, demonstrating that the localization behaviour caused by strain softening is represented very well in the plastic-damage model.

At time C, the next excursion in the downstream direction, Figure 7(c) shows that another horizontal crack forms at the upstream face and quickly joins with the previously formed downstream crack. After the two

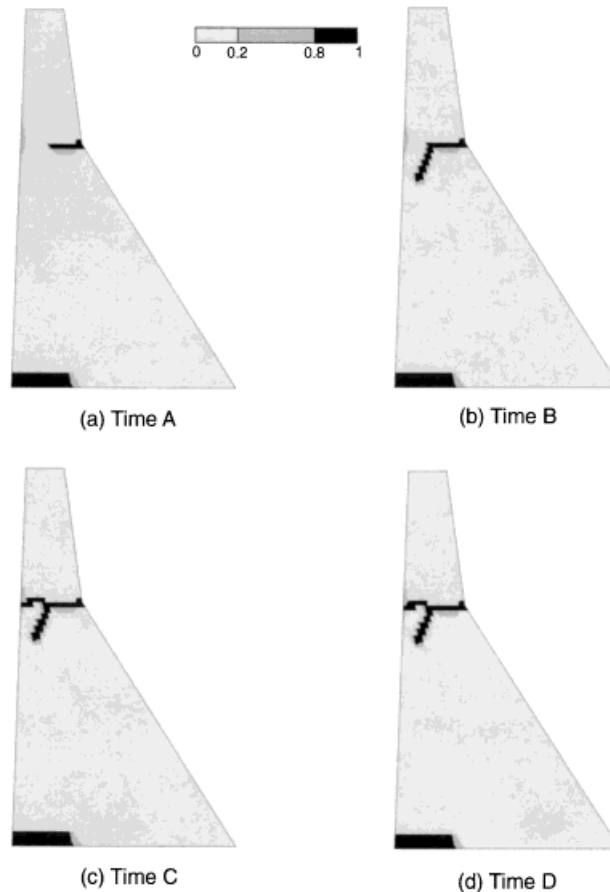
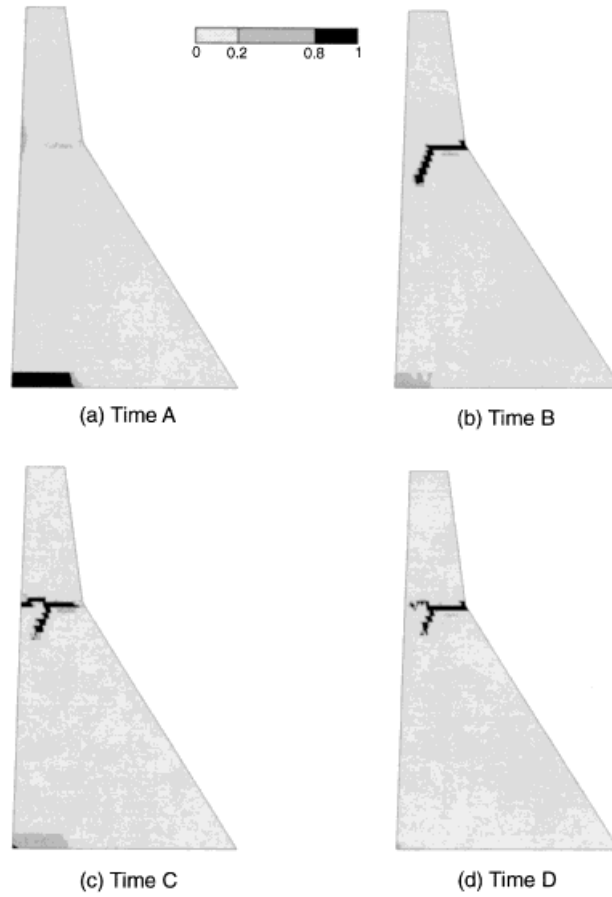
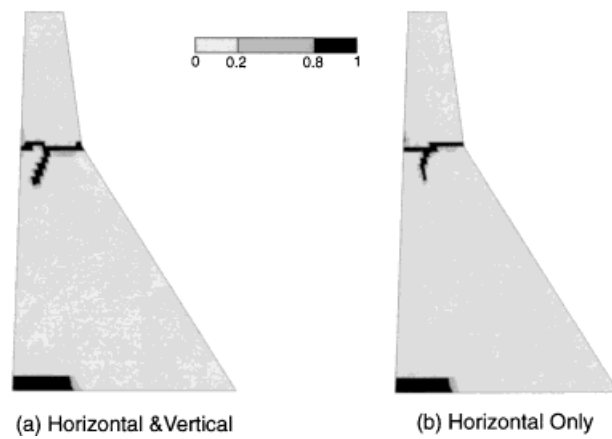


Figure 7. Evolution of tensile damage variable (κ_t)

cracks join, the inclined crack does not propagate further because the tensile stress is now concentrated where the two cracks meet as shown in Figure 6(c). Figure 8(c) shows some recovery of degradation damage near the downstream end of the upper crack as the upper portion of the dam rotates downstream. The crack at the base remains stable and does not propagate further, which is very clear in Figures 8(b) and 8(c) because of the small increase in degradation damage near the base at time C compared with time B.

Finally, at time D as the dam next displaces downstream primarily by rigid body rotation of the upper portion, the upper cracks remain stable as shown in Figure 7(d). The two upstream face cracks close and recover most of the stiffness as shown in Figure 8(d). Subsequent vibration of the dam beyond time D does not substantially change the amount and distribution of damage.

Figure 9 shows the effect of the vertical ground motion component on cracking in the form of contours for the tensile damage variable at 10 secs. Comparing Figure 9(a) with Figure 7(d) confirms that the cracks remain stable under both components of the ground motion. When the dam is subjected to the horizontal component only, the major crack pattern in Figure 9(b) appears qualitatively similar to the cracks in Figure 9(a). There is a difference, however, because in Figure 9(b) the horizontal crack initiated at the downstream face turns down nearly vertically. Subsequently, the upstream crack is arrested when it intersects the previously formed downstream face crack. Although difficult to discern, the tensile damage parameter is smaller and cracking is narrower for Figure 9(b) than for Figure 9(a). The difference in the vertical crack

Figure 8. Evolution of degradation damage variable (D)Figure 9. Effect of vertical ground motion component on tensile damage variable (κ_t) after 10 sec of earthquake response

pattern leads to the phenomenon in Figure 5(b) in which the horizontal ground motion alone does not induce as much rigid body rotation of the upper block as do the combined components.

The effect of the rate-dependent regularization on mesh-objectivity is illustrated in Figure 10. Mesh B in Figure 10(a) is a finer mesh (1710 elements) than mesh A (760 elements). The two meshes are analyzed for both ground motion components with $\mu = 0.15\Delta t = 0.00075$ sec. The characteristic length in the rate-independent backbone model is set to the size of each element for all cases. The horizontal displacements at the dam crest are compared in Figure 10(c), which shows fairly objective results for the two meshes. The contour of tensile damage for the finer mesh at 10 sec in Figure 10(b) is similar to the corresponding result in Figure 9(a), although the crack bandwidth is smaller because of the smaller element size in Mesh B. To examine the effect of the rate dependent regularization, the same meshes are tested without any viscoplastic effect ($\mu = 0$). Figure 10(d) shows that without the rate-dependent regularization, the use of only the characteristic length provides relatively poor objectivity for the mesh size.

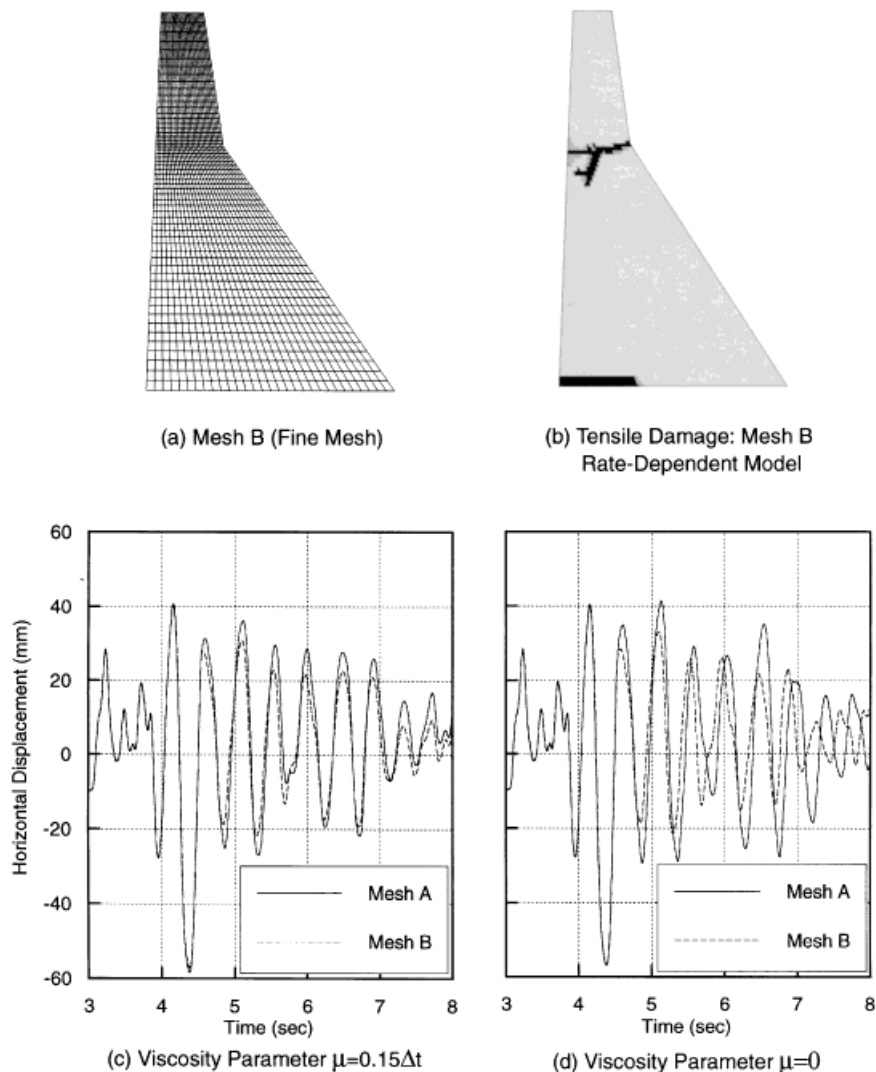


Figure 10. Effect of rate-dependent regularization on mesh objectivity

For the Koyna dam analysis, the convergence rate for the solution of equation (35) was super-linear. The slight loss of the quadratic convergence rate, which is supposed to be obtained with the algorithmic tangent, is mainly due to the residual errors in the stress computation procedure and the C^0 -continuous functions such as r and s . The solution for the 1596 degree-of-freedom mesh A for 3000 time steps takes 60 min of CPU time on a 8 Mflops workstation computer. This is an efficient numerical solution for obtaining such detailed damage information from the constitutive model.

6. CONCLUSIONS

A new plastic-damage constitutive model for cyclic loading of concrete has been applied to the earthquake analysis of concrete gravity dam monoliths. A cyclic rate-independent model is the backbone model for a rate-dependent viscoplastic extension. The constitutive model objectively represents localization of damage caused by strain softening. Large crack opening and subsequent closing is accurately tracked. Damping is consistently accounted for using the reduced stiffness caused by damage degradation. The model replicates cyclic test data on concrete very well.

Since Koyna dam in the 1967 Koyna earthquake is one of the few examples of cracking in a concrete dam, the new plastic-damage model is used to investigate its earthquake response. The evolution of damage in the dam during the earthquake is consistent with the observed cracking in the dam. After cracks form near the change in downstream slope at both faces, the upper portion of the dam rocks nearly as a rigid body. The vertical ground motion is important in the post-cracking response of Koyna dam.

The plastic-damage model is an improvement on the models used in previous studies of dams for several reasons. The inclusion of inelastic strain and multiple damage evolution of the failure criteria (yield surface) traces the history of damage in tension and, although less important for dams, in compression. Degradation of stiffness and subsequent recovery upon crack closing is represented in a consistent manner for simulating both microcracks and large discrete cracks. The use of a rate-dependent constitutive model is important for regularizing a problem that would be ill-posed using a rate-independent model. The present study shows that the characteristic length cannot provide a good mesh objective result unless the (viscoplastic) rate-dependent regularization is used. The rate-dependent regularization scheme also provides excellent representation of the localization of damage caused by cracking. Finally, viscoelastic damping in the dam is represented in a simple but physically realistic manner. Damping is included consistently in the numerical solution by computing the varying restoring force and modifying the algorithmic tangent to maintain optimal convergence to the solution.

Future work includes the implementation of the model for three-dimensional stress states, so it will be suitable for damage and failure analysis of arch dams. Since the constitutive model is formulated for three-dimensions, the implementation does not entail additional considerations except for singularities in the yield surface. More work is possible on calibration and sensitivity of the parameters in the model using additional cyclic test data for concrete. Finally, the influence of viscosity on the characteristic length needs to be studied to improve the objectivity of the finite element solutions.

ACKNOWLEDGEMENTS

This work has been supported by the U.S. Bureau of Reclamation, under Agreement No. 1425-5-FC-81-08970. The authors wish to thank Mr. Larry Nuss for his support.

REFERENCES

1. A. K. Chopra, 'Earthquake response analysis of concrete dams', in R.B. Jansen (e.d), *Advanced Dam Engineering for Design, Construction, and Rehabilitation*, Van Nostrand Reinhold, New York, 1988, pp. 416–465.
2. A. Niwa and R. W. Clough, 'Shaking table research on concrete dam models', Report No. UCB/EERC 80-5, Earthquake Engineering Research Center, University of California, Berkeley, CA, 1980.
3. J. F. Hall, 'The dynamic and earthquake behavior of concrete dams', *Soil Dyn. Earthquake Engng.* **7**, 58–121 (1988).

4. A. K. Chopra and P. Chakrabarti, 'The Koyna earthquake and damage to Koyna dam', *Bull. Seismol. Soc. Amer.* **63**, 381–397 (1973).
5. National Research Council, *Earthquake Engineering for Concrete Dams: Design, Performance, and Research Needs*, National Academy Press, 1990.
6. M. L. Ayari and V. E. Saouma, 'A fracture mechanics based seismic analysis of concrete gravity dams using discrete cracks', *Engng. Fracture Mech.* **35**, 587–598 (1990).
7. N. Pal, 'Seismic cracking of concrete gravity dams', *J. Struct. Div. ASCE* **102**, 1827–1844 (1976).
8. L. Vargas-Loli and G. Fenves, 'Effects of concrete cracking on earthquake response of dams', *Earthquake Engng. Struct. Dyn.* **18**, 575–592 (1989).
9. B. El-Aidi and J. F. Hall, 'Nonlinear earthquake response of concrete gravity dams, part 1: modeling; part 2: behavior', *Earthquake Engng. Struct. Dyn.* **18**, 837–865 (1989).
10. Z. P. Bazant and B. H. Oh, 'Crack band theory for fracture of concrete', *Mater. Struct. (RILEM, Paris)*, **16**, 155–177 (1983).
11. J. G. Rots, 'Computational modeling of concrete fracture', *Ph.D. Dissertation*, Department of Civil Engineering, Delft University of Technology, Delft, 1988.
12. N. Bicanic, R. de Borst, W. Gerstle, D. W. Murry, G. Pijaudier-Cabot, V. Saouma, K. J. Willam and J. Yamazaki, 'Computational aspects', in J. Isenberg (ed.), *Finite Element Analysis of Reinforced Concrete Structures II*, ASCE, New York, 1993, pp. 367–489.
13. S. S. Bhattacharjee and P. Léger, 'Seismic cracking and energy dissipation in concrete gravity dams', *Earthquake Engng. Struct. Dyn.* **22**, 991–1007 (1991).
14. F. Ghrib and R. Tinawi, 'An application of damage mechanics for seismic analysis of concrete gravity dams', *Earthquake Engng. Struct. Dyn.* **24**, 157–173 (1995).
15. M. Cervera, J. Oliver and R. Faria, 'Seismic evaluation of concrete dams via continuum damage models', *Earthquake Engng. Struct. Dyn.* **24**, 1225–1245 (1995).
16. M. Cervera, J. Oliver and O. Manzoli, 'A rate-dependent isotropic damage model for the seismic analysis of concrete dams', *Earthquake Engng. Struct. Dyn.* **25**, 987–1010 (1996).
17. J. Lee and G. L. Fenves, 'A plastic-damage model for cyclic loading of concrete structures', *J. Engng Mech. ASCE*, accepted, Aug. 1998.
18. J. Lubliner, J. Oliver, S. Oller and E. Onate, 'A plastic-damage model for concrete', *Int. J. Solids Struct.* **25**, 299–326 (1989).
19. W. F. Chen and D. J. Han, *Plasticity for Structural Engineers*, Springer, New York, 1988.
20. J. Oliver, 'A consistent characteristic length of smeared cracking models', *Int. J. Numer. Meth. Engng.* **28**, 461–474 (1989).
21. J. Lee, Theory and implementation of plastic-damage model for concrete structures under cyclic and dynamic loading, *Ph.D. Dissertation*, Department of Civil and Environmental Engineering, University of California, Berkeley, CA, 1996.
22. R. L. Taylor, 'FEAP: a finite element analysis program for engineering workstations', *Report No. UCB/SEMM-92 (Draft Version)*, Department of Civil Engineering, University of California, Berkeley, CA, 1992.
23. I. D. Karsan and J. O. Jirsa, 'Behavior of concrete under compressive loadings', *J. Struct. Div. ASCE* **95**, 6935–2563 (1969).
24. V. S. Gopalaratnam and S. P. Shah, 'Softening response of plain concrete in direct tension', *ACI J.* **3**, 310–323 (1985).
25. A. Needleman, 'Material rate dependence and mesh sensitivity in localization problems', *Comput. Meth. Appl. Mech. Engng.* **67**, 69–85 (1988).
26. D. Bigoni and T. Hueckel, 'Uniqueness and localization — I. Associative and non-associative elastoplasticity', *Int. J. Solids Struct.* **28**, 197–213 (1991).
27. M. K. Neilsen and H. L. Schreyer, 'Bifurcation in elasto-plastic materials', *Int. J. Solids Struct.* **30**, 521–544 (1993).
28. I. S. Sandler and T. A. Pucik, 'Non-uniqueness in dynamic rate-independent non-associated plasticity', in G. Z. Voyiadjis *et al.* (eds), *Mechanics of Materials and Structures*, Elsevier, New York, Amsterdam, 1994, pp. 221–240.
29. P. Perzyna, 'Fundamental problems in visco-plasticity', in *Recent Advances in Applied Mechanics*, Academic Press, New York, 1966.
30. G. Duvaut and J. L. Lions, *Inequalities in Mechanics and Physics* (translated from the French by C. W. John), Springer, New York, 1976.
31. J. C. Simo, J. G. Kennedy and S. Govindjee, 'Non-smooth multisurface plasticity and viscoplasticity: loading/unloading conditions and numerical algorithm', *Int. J. Numer. Meth. Engng.* **26**, 2161–2185 (1988).
32. J. Lubliner, *Plasticity Theory*, Macmillan, New York, 1990.
33. R. Hill, 'A general theory of uniqueness and stability in elastic-plastic solids', *J. Mech. Phys. Solids* **6**, 236–249 (1958).
34. B. Loreto and J. H. Prevost, 'Dynamic strain localization in elasto-(visco-)plastic solids, part 1. General formulation and one-dimensional examples', *Comput. Meth. Appl. Mech. Engng* **83**, 247–273 (1990).
35. L. J. Sluys and R. de Borst, 'Wave propagation and localization in a rate-dependent cracked medium - model formulation and one-dimensional examples', *Int. J. Solids Struct.* **29**, 2945–2958 (1992).
36. G. L. Fenves and A. K. Chopra, 'Earthquake analysis of concrete gravity dams including reservoir bottom absorption and dam-water-foundation rock interaction', *Earthquake Engng. Struct. Dyn.* **12**, 663–680 (1984).
37. J. C. Simo, 'Algorithm for static and dynamics multiplicative plasticity that preserve the classical return mapping schemes of the infinitesimal theory', *Comput. Meth. Appl. Mech. Engng* **99**, 61–112 (1992).
38. H. M. Hilber, T. J. R. Hughes and R. L. Taylor, 'Improved numerical dissipation for time integration algorithms in structural dynamics', *Earthquake Engng. Struct. Dyn.* **5**, 283–292 (1977).
39. J. C. Simo and R. L. Taylor, 'Consistent tangent operators for rate-independent elastoplasticity', *Comput. Meth. Appl. Mech. Engng.* **48**, 101–118 (1985).
40. J. W. Ju, 'On energy-based coupled elastoplastic damage theories: constitutive modeling and computational aspects', *Int. J. Solids Struct.* **25**, 803–833 (1989).
41. N. R. Hansen and H. L. Schreyer, 'A thermodynamically consistent framework for theories of elastoplasticity coupled with damage', *Int. J. Solids Struct.* **31**, 359–389 (1994).